Self-Assembly of Gradient Concentric Rings via Solvent Evaporation from a Capillary Bridge

Jun Xu,[1] Jianfeng Xia,[1,2] Suck Won Hong,[1] Zhiqun Lin,[1,*] Feng Qiu,[2] and Yuliang Yang[2]
[1]*Department of Materials Science and Engineering, Iowa State University, Ames, Iowa 50011, USA*
[2]*Department of Macromolecular Science, Fudan University, Shanghai 200433, China*
(Received 11 November 2005; published 13 February 2006)

A drop of solution containing nonvolatile solute is allowed to evaporate from a sphere-on-flat geometry. Left behind is a striking pattern of *gradient* concentric rings with unprecedented regularity. The center-to-center distance between adjacent rings, $\lambda_{C\text{-}C}$, and the height of the ring, h_d, are strongly affected by the concentration of the solution and the properties of the solvent. The nature of the formation of regular gradient ring patterns during the course of irreversible solvent evaporation is revealed through theoretical calculations based on the mass conservation of the solution.

DOI: 10.1103/PhysRevLett.96.066104 PACS numbers: 68.03.Fg

Dynamic self-assembly of nonvolatile solutes through irreversible solvent evaporation of a droplet (*unbound liquid*) is widely recognized as a nonlithography route to produce intriguing patterns [1–10]. Two main characteristic patterns are known. The best studied is produced by temperature-gradient-induced Marangoni-Bénard convection [8–10], which results in irregular polygonal network structures from an upward flow of the warmer lower liquid. The second is the ''coffee ring'' pattern [1–3], which forms when the contact line of an evaporating droplet becomes pinned, ensuring that liquid evaporating from the edge is replenished by liquid from the interior, so that outward flow carries the nonvolatile element to the edge. A subset of the coffee ring phenomena is the concentric ring formed by repeated pinning and depinning events (i.e., stick-slip motion) of the contact line [11–13]. However, stochastic concentric rings (i.e., irregular rings) are generally formed [11]. Moreover, the bulk of theoretical work within lubrication approximation has centered on understanding a *single* ring formation [3,14,15]. Only very few elegant theoretical studies have focused on periodic multiring (i.e., concentric rings) formation during droplet evaporation on a single surface [11,12].

To date, a few attempts have been made to control a droplet evaporation in a confined geometry (*bound liquid*) [6,16,17]. Recently, a periodic family of concentric ring patterns with unprecedented regularity has been produced by constraining a drop of polymer solution in a confined geometry composed of either two cylindrical mica surfaces placed at a right angle to one another [16] or a sphere on a flat surface [17]. However, the nature of the formation of such highly regular patterns remains to be addressed.

In this Letter, we report *gradient* concentric ring patterns formed from a capillary-held polymer solution in a confined geometry consisting of a spherical lens on a silicon surface (sphere on Si) as illustrated in Fig. 1(a). The concentration of the solution and the properties of the solvent are found to exert profound influences on the center-to-center distance between adjacent rings ($\lambda_{C\text{-}C}$) and the height of the ring (h_d). Each ring is nanometers in height and microns wide. Both $\lambda_{C\text{-}C}$ and h_d decrease slowly with increasing proximity to the center of the sphere/Si contact (Fig. 1). In other words, the patterns are gradient [Fig. 1(b)]. A theoretical calculation based on mass conservation of the solution is conducted for the first time to gain physical insight of the pattern formation and agrees well with the experimental observations.

A linear conjugated polymer, poly[2-methoxy-5-(2-ethylhexyloxy)-1,4-phenylenevinylene] (MEH-PPV) (MW = 50–300 kg/mole) was selected as nonvolatile solute. The choice of system was motivated by its numerous potential applications in the areas of light emitting diode, photovol-

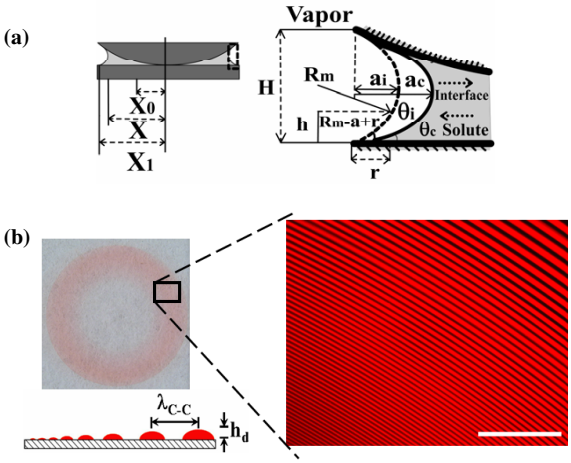

FIG. 1 (color online). (a) *Left*: Schematic cross section of a capillary-held solution containing nonvolatile solute placed in a sphere-on-flat configuration. X_1, X, and X_0 are the radii of outermost, intermediate, and innermost rings from the center of sphere/flat contact, respectively. *Right*: The close-up of the capillary edge marked in the left panel. The parameters used in the calculation are illustrated. (b) The digital image of entire gradient concentric ring patterns formed by the deposition of the solute (i.e., MEH-PPV from the 0.075 mg/ml toluene solution) in the geometry in (a). On the right side, a small zone of the fluorescent image of MEH-PPV ring patterns is shown. The scale bar is 200 μm. As the solution front moves inward, rings become smaller and the height decreases as illustrated in lower left schematic.

taic cells, thin-film transistors, and biosensors [18]. An additional advantage of employing MEH-PPV is that it enables fluorescence imaging. Therefore we were able to confirm that no MEH-PPV was deposited between adjacent rings [Fig. 1(b)]. Two MEH-PPV toluene solutions were prepared at concentrations $c = 0.075$ and 0.05 mg/ml, respectively. The MEH-PPV benzene and chlorobenzene solutions were also prepared at $c =$ 0.03 mg/ml. A drop of 12 μL solution was loaded between the spherical lens (the radius of curvature is 2 cm) and the Si surface. Subsequently, two surfaces were brought into contact with inchworm motor so that a capillary-held MEH-PPV solution (capillary bridge) was formed with the evaporation rate highest at the edge of the drop [Fig. 1(a)] [16,17]. Experiments were performed at room temperature inside a homemade chamber so that the evaporation rate of the solvent was *controlled* and temperature gradient was eliminated. The pattern formation was monitored *in situ* by optical microscopy (OM).

The *in situ* OM observation revealed that the contact line of the droplet moved in a controlled, repetitive stick-slip fashion [i.e., a competition between pining force and depinning force (capillary force)] [11–13] toward the center of the sphere/Si contact with elapsed time (see the real-time lapse video in supporting information [19]). A dark front (i.e., meniscus) was clearly evident at the capillary edge. The solution front (i.e., liquid-vapor interface) was arrested at the spherical lens and Si surfaces for a certain period of time during which a MEH-PPV ring was formed. Then it jumped a short distance to the next position where it was arrested again and a new ring was thus deposited. The jumping distance ($\lambda_{C\text{-}C}$) was found to decrease slowly with increasing proximity to the center of sphere/Si contact.

After the evaporation was complete, the two surfaces were separated and examined by OM and atomic force microscope (AFM). Highly ordered gradient concentric rings (both $\lambda_{C\text{-}C}$ and width) were observed that span almost the entire surfaces of both the spherical lens and Si, except the region where the sphere was in contact with Si, as seen in the digital image [Fig. 1(b)]. Only the patterns on Si were evaluated. The first AFM image (images are all 100×100 μm^2 in the measurements) was taken starting from the outermost ring. Efforts were made to ensure that the ring patterns are perpendicular to the scan direction. Then, the AFM tip was moved toward the sphere/Si contact center by exactly 100 μm using the automated translational stage of the AFM. Subsequently, the second image was captured. The scans and movements were repeated until no rings could be imaged. Finally, the tip was moved to pass the contact center and reach the other end of the ring patterns so that the diameter d of outmost ring could be obtained, which is found to be consistent with the value obtained using a digital camera (In the present study, $d =$ 8500 μm was found for the 0.075 mg/ml toluene solution [Fig. 1(b)].) The data were then processed as follows. Each 100×100 μm^2 image was split into two 50×50 μm^2 scans from the center of the AFM image. The $\lambda_{C\text{-}C}$ and the height of the ring, h_d, were obtained after averaging from 5 cross sections of an AFM image (50×50 μm^2). The center-to-center distance of adjacent rings was measured as $\lambda_{C\text{-}C}$. The absolute position of the ring away from the sphere/Si contact center, i.e., X, was also determined.

Figure 2 shows $\lambda_{C\text{-}C}$ and h_d, obtained from dynamic self-assembly of two MEH-PPV toluene solutions at the different concentrations, as a function of X. As c decreased from 0.075 to 0.05 mg/ml, both $\lambda_{C\text{-}C}$ and h_d reduced. This can be qualitatively rationalized as follows. Compared to the case at $c = 0.075$ mg/ml, there were fewer MEH-PPV with which to create local surface roughness to pin the contact line at lower concentration ($c = 0.05$ mg/ml) [10,20]. The pinning time was therefore much shorter. In other words, the evaporative loss of toluene ΔV was less, which in turn caused the contact line to deposit less (i.e., smaller h_d and width as confirmed by AFM) and to hop less inward to the next position (i.e., smaller $\lambda_{C\text{-}C}$). For example, at $X = 3775$ μm for the 0.05 mg/ml solution, $\lambda_{C\text{-}C}$ is 8.9 μm with 7.1 nm in height [Figs. 2(a) and 2(b)]. However, these values were much larger for $c =$ 0.075 mg/ml ($\lambda_{C\text{-}C} = 12.8$ μm and $h_d = 11.4$ nm). Two representative 3D AFM height images and corresponding profiles, obtained from the 0.075 mg/ml solution, are shown in Figs. 2(a) and 2(b) as insets, respectively. Both $\lambda_{C\text{-}C}$ and h_d decreased from 11.5 μm and 9.5 nm at $X =$ 3725 μm to 7.6 μm and 5.9 nm at $X = 3375$ μm as the evaporation front moved inward. For the 0.075 mg/ml solution, concentric rings are formed from 4250 μm (X_1) to 2625 μm (X_0), where X_1 and X_0 are the radii of outermost and innermost ring in the experiment, respectively. The values of $X_1 = 4250$ μm and $X_0 = 2825$ μm are found for the 0.05 mg/ml solution. It should be noted that, to exclude the possible hydrodynamic instabilities caused when the sphere is brought in contact with the Si surface, the rings formed in the range from 4000 to 4250 μm at the early stage of the evaporation are not analyzed.

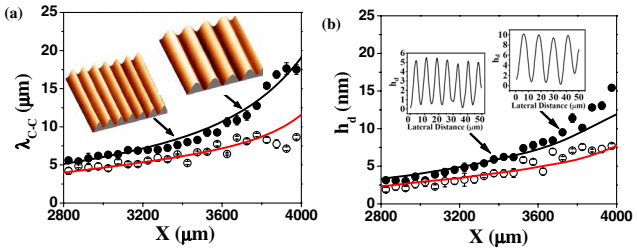

FIG. 2 (color online). Concentration effect. (a) $\lambda_{C\text{-}C}$ and (b) h_d are plotted as a function of X at different concentrations (solid and open circles corresponding to the data obtained from toluene solutions at $c = 0.075$ mg/ml and 0.05 mg/ml, respectively). X is the distance away from the center of sphere/Si contact. Two representative 3D AFM topographical images (50×50 μm^2) and the corresponding cross sections obtained from the 0.075 mg/ml solution are given as insets in (a) and (b), respectively.

The amount of volume loss of the solvent ΔV is governed by the competition between pinning force and capillary force. The pinning force is proportional to the total length of the contact line [$\sim 2\pi X$ in Fig. 1(a)] [20], which decreases linearly in the course of the stick-slip motion of the contact line. The capillary force $F_C = 16\pi\gamma_{lv}X \times \arctan(4aR/X^2)$, however, is nonlinear, where γ_{lv} is the surface tension of the solvent, and a and R are the height of meniscus and the radius of curvature of the spherical lens, respectively [Fig. 1(a)]. The imbalance between linear pinning force and nonlinear capillary force resulted in a nonlinear ΔV. Consequently, the patterns were gradient rather than strictly repetitive.

To quantitatively uncover the nature of the formation of concentric rings exhibiting gradient in both $\lambda_{C\text{-}C}$ and h_d, we performed a theoretical calculation based on the mass conservation during the course of the solvent evaporation. As toluene evaporates, MEH-PPV jams into the edge of the solution next to the contact line, preventing it from retracting (i.e., ''stick''). The chemical property of deposited MEH-PPV is different from the sphere and Si. The deposition (jamming) creates local surface roughness at sphere and Si surfaces. Both chemical inhomogeneities and surface roughness contribute to the pinning of the contact line [20]. During the deposition of MEH-PPV the initial contact angle θ_i decreases gradually, owing to the evaporative volume loss of toluene ΔV to a critical angle θ_C [Fig. 1(a)] at which the capillary force becomes larger than the pinning force [2,3,14,15,21]. This leads the contact line to jump to a new position (i.e., ''slip''). The ΔV during the formation of MEH-PPV ring (i.e., a changing from a_i to a_c) is given by

$$\Delta V = \pi X H\left\{H\left[\arctan\left(\frac{2a_c}{H}\right) - \arctan\left(\frac{2a_i}{H}\right)\right] + (a_c - a_i)\right\}, \tag{1}$$

where H is the surface separation at the liquid-vapor interface of the solution, and a_i and a_c are the height of meniscus at contact angles θ_i and θ_C, respectively. The relation of θ and a can be established from the geometry of capillary edge defined in Fig. 1(a).

$$\left(\frac{H}{2} - h\right)^2 + (R_m - a + r)^2 = R_m^2, \tag{2}$$

$$\theta \approx \tan\theta = \left.\frac{\partial h}{\partial r}\right|_{x=0} \approx \frac{H - 2a}{H}, \tag{3}$$

where R_m is the radius of curve of the capillary edge ($H \approx 2R_m$), h is the local thickness of capillary edge at the position r, and $H \approx \frac{X^2}{2R}$. The volume of confined solution V_{Liq} [i.e., light gray area in Fig. 1(a)] is

$$V_{\text{Liq}} = \pi X^2 H - \pi R H^2 - \pi X H^2 \arctan\frac{2a}{H} + \frac{\pi X H^2}{2} - \pi X a H \tag{4}$$

and

$$V_{\text{Liq}}^{\text{new}} = V_{\text{Liq}} - \Delta V. \tag{5}$$

The initial contact angle θ_i is $\sim 18°$, calculated from Eqs. (3) and (4) since the initial loading volume V_{Liq} and initial X (i.e., X_1) are known from the experiment. It agrees well with the value determined experimentally from the side view of the capillary edge using a digital camera [22]. Combining Eqs. (1) and (3)–(5), the new position X_{new}, at which a contact line is arrested, can be identified by iterative calculation until a best fit [lines in Fig. 2(a)] with experimental data [symbols in Fig. 2(a)] is reached [23]. The calculated outermost $\lambda_{C\text{-}C} = X_1 - X$ and subsequent $\lambda_{C\text{-}C} = X - X_{\text{new}}$ can thus be obtained.

In the lubrication approximation after considering the evaporation process, the evolution equation of the local thickness of capillary edge is given by [3,12,15]

$$\rho\frac{dh}{dt} = -\rho\frac{1}{r}\frac{d}{dr}(rhv) - J, \tag{6}$$

where ρ is the density of the solvent ($\rho \approx 1$), and J is the mass of solvent evaporating per unit area unit time and assumed to be a constant. The average velocity of the solute moving toward the capillary edge to pin the contact line as illustrated in Fig. 1(a) can be obtained by the integration of Eq. (6) [24]:

$$v(r,t) = \left[-\frac{r}{2\rho h}J + \frac{1}{h\rho r}\frac{(4J\arctan\frac{2a}{H})(H^2 + 4a^2)}{(3H^2 + 4a^2)}Q\right]. \tag{7}$$

When the time $t = r/v$ is smaller than the pinning time t_p, the solute is allowed to transport, deposit, and form a ring at the contact line with a height h_d (assuming that the cross section of the ring is a cylindrical ridge in one dimension), which can be calculated by

$$h_d = \left[\frac{V_{\text{deposit}}}{2\pi X(\alpha - \cos\alpha\sin\alpha)}\right]^{1/2}(1 - \cos\alpha), \tag{8}$$

where α is the angle between the ring and the Si surface ($a \approx 0.5°$ estimated based on AFM image). V_{deposit} is the volume of deposits formed during the pinning time and calculated by

$$V_{\text{deposits}} = \frac{c}{\rho_d}\int_0^r 2\pi X h dr, \tag{9}$$

where c is concentration of the solution, ρ_d is the density of the deposited solute ($\rho_d \approx 1$).

The solid lines in Fig. 2 represent the calculated values of $\lambda_{C\text{-}C}$ and h_d based on the mass conservation discussed above, yielding θ_C of 15.6° and 16.1° for MEH-PPV solutions at $c = 0.075$ mg/ml and $c = 0.05$ mg/ml, respectively. Good agreement between experimental data and theoretical fits is clearly evident. The pinning force is directly related to the surface roughness [20]. An increase in h_d during MEH-PPV deposition results in a decrease in θ_C [3,15,20,21]. A smaller θ_C implies a longer pinning time t_p, which in turn causes a greater volume loss ΔV during pinning. As a result, it leads to a larger pull away of the contact line to reach initial contact angle θ_i at a

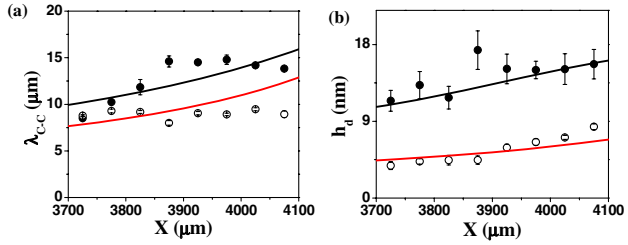

FIG. 3 (color online). Solvent effect. (a) $\lambda_{C\text{-}C}$ and (b) h_d are plotted as a function of X with different solvents employed. The solid and open circles are data from 0.03 mg/ml benzene and 0.03 mg/ml chlorobenzene solutions, respectively.

new position. Thus, a larger $\lambda_{C\text{-}C}$ was observed at $c = 0.075$ mg/ml as shown in Fig. 2(a).

Figure 3 illustrates quantitative differences in $\lambda_{C\text{-}C}$ and h_d as different solvents (benzene and chlorobenzene) were used. The concentration of both MEH-PPV solutions is 0.03 mg/ml. The boiling point (T_b) of benzene and chlorobenzene are 80 and 130 °C, respectively, which implies that benzene evaporates faster than chlorobenzene (i.e., a faster evaporation rate J for benzene). Thus, larger volume loss ΔV is expected for the MEH-PPV benzene solution to reach θ_C and hop to the next position inward. Accordingly, a larger $\lambda_{C\text{-}C}$ would result as is evidenced in Fig. 3(a). For benzene solution ($X_1 = 4125$ μm and $X_0 = 3675$ μm were found in the experiment) the number of concentric rings formed is much fewer than that from chlorobenzene solution ($X_1 = 4275$ μm and $X_0 = 2925$ μm) as a result of faster evaporation of benzene. To render a meaningful comparison, only the data points in the region of 3700–4100 μm are presented in Fig. 3. The ΔV is dominantly dictated by θ_i and θ_C [Eqs. (1) and (3)]. The fitting of the experimental values of $\lambda_{C\text{-}C}$ yields $\theta_i = 35°$ and $\theta_C = 32°$ for the MEH-PPV benzene solution, and $\theta_i = 16°$ and $\theta_C = 14°$ for the MEH-PPV chlorobenzene solution. The larger difference between θ_i and θ_C for the benzene solution ($\Delta\theta = 3°$) signifies a greater ΔV, suggesting that more MEH-PPV are deposited, reflected as higher value of h_d observed in the experiment [Fig. 3(b)] and the solution front would retract at a bigger pace subsequently. Thus, larger $\lambda_{C\text{-}C}$ and h_d are obtained in the case of the MEH-PPV benzene solution.

In conclusion, we showed that gradient concentric ring patterns of high regularity could form spontaneously, simply by allowing a droplet to evaporate in a consecutive stick-slip motion in a confined geometry. The use of solutions with different concentrations and different solvents effectively mediated the evaporative loss of the solvent and the deposition time of the solute, thereby affecting $\lambda_{C\text{-}C}$ and h_d. A simple theoretical calculation has, for the first time, been performed to reveal the nature of the formation of gradient ring patterns. The studies demonstrate that dynamic self-assembly in a confined geometry may offer a new means to produce gradient features, as well as a simple, versatile, generalizable approach to produce yet more complex patterns. This natural, pattern-forming process could find use in fields such as nanotechnology and optoelectronics.

We gratefully acknowledge the support from the American Chemical Society Petroleum Research Fund (Grant No. 42825-G7) and the 3M Grant. We also thank Vladimir Tsukruk for helpful discussions.

*To whom correspondence should be addressed.
Electronic address: zqlin@iastate.edu

[1] R. D. Deegan *et al.*, Nature (London) **389**, 827 (1997).
[2] R. D. Deegan, Phys. Rev. E **61**, 475 (2000).
[3] R. D. Deegan *et al.*, Phys. Rev. E **62**, 756 (2000).
[4] O. Karthaus, L. Grasjo, N. Maruyama, and M. Shimomura, Chaos **9**, 308 (1999).
[5] P. G. de Gennes, Eur. Phys. J. E **7**, 31 (2002).
[6] H. Yabu and M. Shimomura, Adv. Funct. Mater. **15**, 575 (2005).
[7] E. Rabani, D. R. Reichman, P. L. Geissler, and L. E. Brus, Nature (London) **426**, 271 (2003).
[8] S. Q. Xu and E. Kumacheva, J. Am. Chem. Soc. **124**, 1142 (2002).
[9] Z. Mitov and E. Kumacheva, Phys. Rev. Lett. **81**, 3427 (1998).
[10] V. X. Nguyen and K. J. Stebe, Phys. Rev. Lett. **88**, 164501 (2002).
[11] E. Adachi, A. S. Dimitrov, and K. Nagayama, Langmuir **11**, 1057 (1995).
[12] M. Nonomura *et al.*, J. Phys. Soc. Jpn. **72**, 2468 (2003).
[13] L. Shmuylovich, A. Q. Shen, and H. A. Stone, Langmuir **18**, 3441 (2002).
[14] Y. O. Popov, Phys. Rev. E **71**, 036313 (2005).
[15] B. J. Fisher, Langmuir **18**, 60 (2002).
[16] Z. Q. Lin and S. Granick, J. Am. Chem. Soc. **127**, 2816 (2005).
[17] S. W. Hong *et al.*, Chem. Mater. **17**, 6223 (2005).
[18] B. J. Schwartz, Annu. Rev. Phys. Chem. **54**, 141 (2003).
[19] See EPAPS Document No. E-PRLTAO-96-089607 for a movie of evaporation induced self-assembly. For more information on EPAPS, see http://www.aip.org/pubservs/epaps.html.
[20] P. G. de Gennes, Rev. Mod. Phys. **57**, 827 (1985).
[21] Y. O. Popov and T. A. Witten, Phys. Rev. E **68**, 036306 (2003).
[22] The θ_i of MEH-PPV benzene and chlorobenzene solutions in the sphere-on-Si geometry are determined in the same way, from both experiment and calculation, yielding $\theta_i = 35°$ and 16°, respectively.
[23] Since X is experimentally measurable, a_i [Eq. (3)] and V_{Liq} [Eq. (4)] can be calculated given that θ_i is known. Similarly, a_c and ΔV are calculated by substituting θ_C so that $V_{\mathrm{Liq}}^{\mathrm{New}}$ [Eq. (5)] can be obtained. Equating Eqs. (4) and (5), the X_{new} is thus yielded.
[24] $Q = \frac{A-B}{4\sqrt{(a-r)(H+r-a)}}$, where $A = (r-a)(11aH - 10a^2 - H^2 + 8ar + Hr + 2r^2)$ and $B = (H-4a)^2 \times \sqrt{(a-r)(H+r-a)}\arctan[\frac{\sqrt{a-r}}{\sqrt{H+r-a}}]$.